

Article

Optimal Design of a High Efficiency LLC Resonant Converter with a Narrow Frequency Range for Voltage Regulation

Junhao Luo ¹, Junhua Wang ¹ , Zhijian Fang ^{1,*} , Jianwei Shao ¹ and Jianguai Li ^{2,*}

¹ School of Electrical Engineering, Wuhan University, Wuhan 430072, China; junhao_l@foxmail.com (J.L.); junhuawang@whu.edu.cn (J.W.); hitwhshao@whu.edu.cn (J.S.)

² School of Mechanical and Electronic Engineering, Wuhan University of Technology, Wuhan 430070, China

* Correspondence: fzj@whu.edu.cn (Z.F.); jianguai@whut.edu.cn (J.L.); Tel.: +86-159-2727-9055 (Z.F.)

Received: 24 March 2018; Accepted: 24 April 2018; Published: 2 May 2018



Abstract: As a key factor in the design of a voltage-adjustable LLC resonant converter, frequency regulation range is very important to the optimization of magnetic components and efficiency improvement. This paper presents a novel optimal design method for LLC resonant converters, which can narrow the frequency variation range and ensure high efficiency under the premise of a required gain achievement. A simplified gain model was utilized to simplify the calculation and the expected efficiency was initially set as 96.5%. The restricted area of parameter optimization design can be obtained by taking the intersection of the gain requirement, the efficiency requirement, and three restrictions of ZVS (Zero Voltage Switch). The proposed method was verified by simulation and experiments of a 150 W prototype. The results show that the proposed method can achieve ZVS from full-load to no-load conditions and can reach 1.6 times the normalized voltage gain in the frequency variation range of 18 kHz with a peak efficiency of up to 96.3%. Moreover, the expected efficiency is adjustable, which means a converter with a higher efficiency can be designed. The proposed method can also be used for the design of large-power LLC resonant converters to obtain a wide output voltage range and higher efficiency.

Keywords: LLC resonant converter; frequency range; optimal design; gain; efficiency

1. Introduction

LLC resonant converters are widely used for their advantages of high efficiency, high power density, easy implementation of magnetic integration, no need for a filter inductor for the output side, and low EMI [1–5]. An LLC resonant converter is required to work efficiently in a certain range of output voltages in many applications, such as charging for electric vehicles or other batteries. However, there is a problem of a wide frequency regulating range [6] for the design of a voltage-adjustable converter, which will lead to increased transformer size and conduction losses [7,8] and is not conducive to the optimization of magnetic components and efficiency improvement [9]. The problems above limit the application of LLC resonant converters in the charging field. Therefore, in the optimal design of an LLC resonant converter, the frequency variation range should be reduced and high efficiency needs to be ensured under the premise of satisfying the required gain.

The frequency-domain analysis method fundamental harmonic approximation (FHA) is a commonly used method to obtain the voltage gain for the design of LLC resonant converters based on the equivalent alternating current (AC) circuit of the resonant tank. However, the accuracy is unsatisfying. Other approaches, such as state-plane [10,11] or time-domain analysis [12,13] rely on the exact model of the converter to provide a precise description of a circuit's behavior. Compared with

the FHA-based method, time-domain analysis can obtain a higher accuracy. Thus, the parameters of the system can be comprehensively considered for the optimization of its design.

Based on the analysis of six different operating modes of an LLC resonant converter in the time-domain model, the frequency-voltage gain distribution and the frequency-output power distribution of each operating mode are obtained by listing the boundary equations between the operating modes [14]. In Reference [15], high efficiency is set as the objective function, and the optimal values of the resonance parameters are solved by computer programming based on time-domain state equations and optimization methods for numerical nonlinear systems. However, due to the multiple combinations of the time-domain modes of an LLC resonant converter and the difficulty involved in obtaining an analytical solution of the boundary conditions under different operating modes, a simplified time-domain analysis model is established in this paper to simplify the design complexity.

In order to optimize the operation frequency range of LLC resonant converters, Reference [16] proposed a design method which limits the maximum working frequency under the condition of meeting the variation range of the output voltage. Nevertheless, it is not fully considered. A method [17] based on full mode time-domain analysis was proposed to achieve different output voltage ranges by combinations of different modes with high accuracy. However, it works in various combinations of modes, which is not conducive to performance optimization of the converter, with an increased complexity of the design process. In Reference [18], a modified LLC converter with two transformers is proposed that can reduce the excitation current while maintaining a high gain range by changing the equivalent magnetizing inductance and turns ratio. Nevertheless, the increased number of transformers lowers the power density. In Reference [9], an LLC resonant converter with a dual resonant frequency is proposed to achieve narrow switching frequency variation. However, the converter added a new pair of small-rated power switches and an auxiliary inductor with an increased volume and cost. Reference [19] presented an optimization method based on operation mode analysis and peak gain placement. Following the approach, the conduction loss can be minimized while maintaining the required gain range. The method can reach 1.455 times the normalized voltage gain in the frequency variation range of about 56 kHz. Reference [20] presented a design method for a high efficiency LLC resonant converter with a wide output voltage. The magnetic components of the converter are optimized based on precise time-domain analysis. The method can reach 1.41 times the normalized voltage gain in the frequency variation range of about 38 kHz.

This paper proposes an optimal design method for LLC resonant converters that can narrow the frequency range and ensure high efficiency under the premise of obtaining the required gain. The paper is organized as follows:

- In Section 2, different operating modes of an LLC resonant converter are analyzed and the optimal working mode is selected. Based on the state equations, a simplified time-domain analysis model is established to obtain the gain curve;
- In Section 3, conditions to achieve ZVS on the primary side from full-load to no-load conditions are studied, through which three restrictions on converter parameters can be obtained;
- In Section 4, to achieve high efficiency LLC resonant converters, the loss and efficiency are calculated. Taking the intersection of the gain requirement, the efficiency requirement, and three restrictions of ZVS, the restricted area of parameter optimization design can be obtained;
- In Section 5, the proposed method is verified by simulation and experiment; and
- The conclusions are given in Section 6.

2. Simplified Gain Model

A full-bridge LLC resonant converter considering the parasitic capacitance is shown in Figure 1, which is composed of a resonant inductor, a resonant capacitor, and a magnetic inductor. C_p and C_s are the equal self-capacitances of the primary and secondary windings, respectively; and C_{ps} is the equal mutual capacitances between the primary and secondary windings. The converter has the

advantages of achieving ZVS on the primary side and ZCS (Zero Current Switch) on the secondary side. Meanwhile, the SRs (Synchronous Rectifier) are used to reduce the conduction losses. Due to these advantages, LLC resonant converters have been widely used in high efficiency and high power density applications.

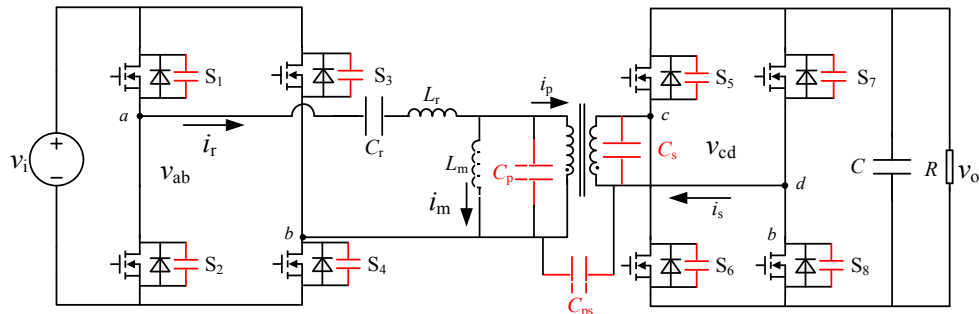


Figure 1. LLC resonant converter circuit considering the parasitic capacitance.

There are four kinds of operating modes (P, PO, PON, and PN) when $f \leq f_r$ (resonant frequency) [19,20] as is displayed in Figure 2. When the switching frequency of the LLC resonant converter equals the resonant frequency, it is called P mode as is shown in Figure 2a. At this mode, only L_r and C_r participate in the resonance, the resonant inductor current i_r is a standard sine wave, and the magnetizing current i_m is a triangular wave.

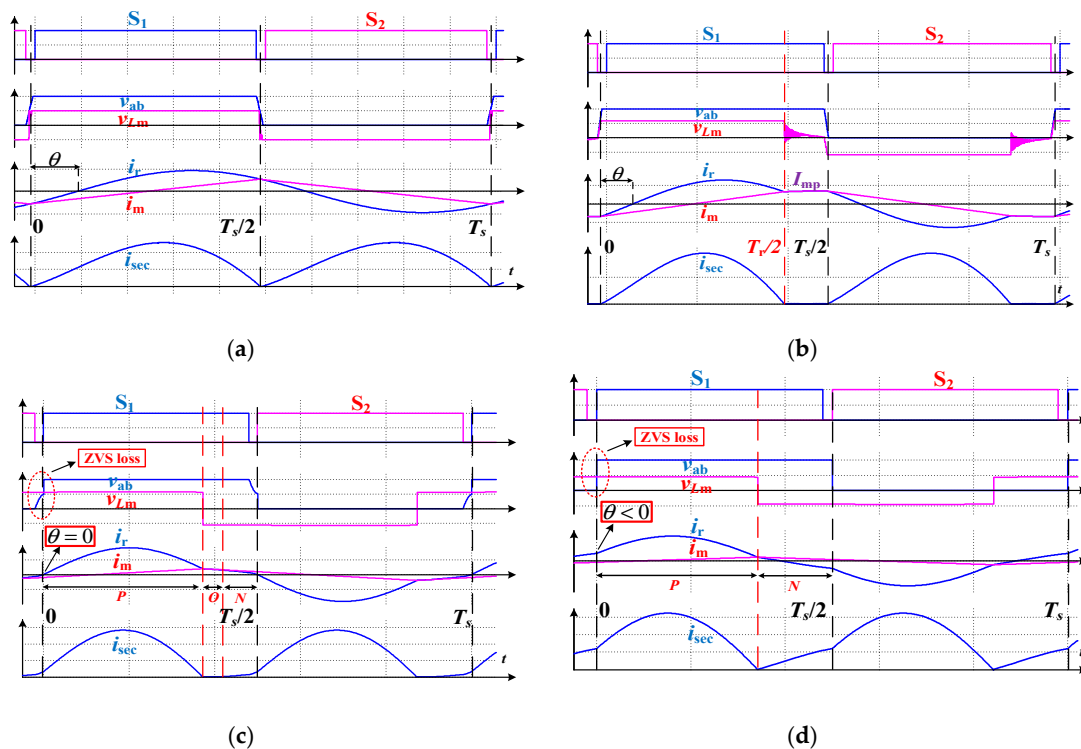


Figure 2. Operating mode division of LLC ($f \leq 1$): (a) P mode($f = 1$); (b) PO mode; (c) PON mode; (d) PN mode.

As is displayed in Figure 2b, the converter works at the PO mode as f decreases. The converter enters the O mode at the end of the P mode when $i_r = i_m$, and the switches on the secondary side cut off. At the O mode, L_m , L_r , and C_r resonate together. The entire PO mode circuit works in the ZVS

region. Meanwhile, the secondary side can achieve ZCS. The PO mode is considered the best working mode [19,20].

When f continues to decrease, the converter enters the PON mode or the PN mode. As can be seen from Figure 2c,d, the two modes have lost their ZVS characteristics and their resonant current lag angle is less than or equal to zero. The PON and PN modes lie in capacitive impedance states. In addition, the relationship between the voltage gain and the switching frequency is no longer monotonous, and closed-loop instability may occur at these modes. According to the above analysis, the designed LLC resonant converter in this paper works at the PO mode.

1. P mode

When the converter works at P mode, Equation (1) can be obtained as follows for the magnetic inductance:

$$nv_o = L_m \frac{di_m}{dt}. \quad (1)$$

It can be obtained from the KCL equation of the LLC resonant converter in half a cycle:

$$\begin{cases} i_r = I_r \sin(2\pi f_r t - \theta_P) \\ i_m = i_m(0) + nv_o \cdot t / L_m \\ i_s = n(i_r - i_m) \\ I_{off} = i_r(0.5T) \\ i_r(0) = i_m(0) \\ i_r(0.5T) = i_m(0.5T) \\ i_r(0) = -i_r(0.5T) \end{cases}. \quad (2)$$

I_{off} represents the off-current of the MOSFET, I_m represents the peak value of the magnetizing current, and θ_P represents the angle that the resonant current lags with voltage v_{ab} .

At P mode, $f_s = f_r$. It can be derived as follows:

$$I_r \sin(\theta_P) = I_m = \frac{nv_o}{4L_m f_r}. \quad (3)$$

2. PO mode

As for the PO mode, when the switching frequency f_s is close to the resonant frequency f_r and the L_m is large, the time of O mode is relatively short and the current change is very small. To simplify the calculation, i_r and i_m can be considered unchanged at O mode. The peak value of the magnetizing current is indicated in Formula (3). The resonance current and magnetizing current can be expressed respectively as:

$$\begin{cases} i_r = \begin{cases} i_{r1}(t) = I_r \sin(2\pi f_r t - \theta_{PO}), 0 \leq t \leq T_r/2 \\ i_{r2}(t) = \frac{nv_o}{4f_r L_m}, T_r/2 < t < T_s/2 \end{cases} \\ i_m = \begin{cases} i_{m1}(t) = nv_o \cdot t / L_m - \frac{nv_o}{4f_r L_m}, 0 \leq t \leq T_r/2 \\ i_{m2}(t) = \frac{nv_o}{4f_r L_m}, T_r/2 < t < T_s/2 \end{cases} \end{cases}. \quad (4)$$

T_s represents the switching cycle at this time. When $t = 0$:

$$i_r(0) = I_r \sin(-\theta_{PO}) = -\frac{nv_o}{4f_r L_m}. \quad (5)$$

During a half-switching period, the average value of the primary current of the transformer and the average value of the secondary current satisfy the relation:

$$\frac{2}{T_s} \int_0^{T_s/2} |n(i_r - i_m)| dt = I_o. \quad (6)$$

According to Formulas (3)–(6):

$$I_r \cos(\theta_{PO}) = \frac{\pi I_o f_r}{2n f_s} \quad (7)$$

$$\begin{cases} \theta_{PO} = \arctan\left(\frac{n^2 v_o}{2\pi f_r I_o L_m} \cdot \frac{f_s}{f_r}\right) = \arctan\left(\frac{n^2 R}{2\pi f_r L_m} \cdot \frac{f_s}{f_r}\right) \\ I_r = \sqrt{\left(\frac{n v_o}{4f_r L_m}\right)^2 + \left(\frac{\pi I_o f_r}{2n f_s}\right)^2} = \sqrt{\left(\frac{n v_o}{4f_r L_m}\right)^2 + \left(\frac{\pi v_o f_r}{2n R f_s}\right)^2} \end{cases} \quad (8)$$

When $f_s = f_r$, the effective value of the original and secondary resonant currents of the converter is shown in Formula (9).

$$\begin{aligned} I_{r,f_r} &= \sqrt{\left(\frac{n v_o}{4f_r L_m}\right)^2 + \left(\frac{\pi I_o}{2n}\right)^2} = \sqrt{\left(\frac{n v_o}{4f_r L_m}\right)^2 + \left(\frac{\pi v_o}{2n R}\right)^2} \\ I_{r,f_r,RMS} &= I_{r,f_r} / \sqrt{2} \\ I_{s,f_r,RMS} &= \sqrt{\frac{2}{T_r} \int_0^{T_r/2} (n(i_r - i_m))^2 dt} = \frac{\sqrt{3}}{24\pi} \sqrt{(5\pi^2 - 48) \left(\frac{n^2 v_o}{4f_r L_m}\right)^2 + 12 \left(\frac{\pi^2 v_o}{R}\right)^2} \end{aligned} \quad (9)$$

At P mode, the magnetizing inductance is clamped at the output voltage. The corresponding state equation is:

$$\begin{cases} v_i - v_{C_{r1}}(t) - L_r \frac{d}{dt} i_{r1}(t) = n v_o \\ C_r \frac{d}{dt} v_{C_{r1}}(t) = i_{r1}(t) \end{cases} \quad (10)$$

At O mode, the secondary diode turns off naturally, and it can be considered approximately that the inductor current is unchanged and the voltage of the resonant capacitor increases linearly. The corresponding state equation is:

$$C_r \frac{d}{dt} v_{C_{r2}}(t) = i_{r2}(t) = i_{m2}(t). \quad (11)$$

According to the continuity of the signal at the P and O modes and the symmetry of the voltage of the resonant capacitor, it can be derived that:

$$v_o = v_i + \frac{n v_o}{4L_m C_r} (T_s - T_r). \quad (12)$$

The normalized gain expression is given after simplifying Formula (12):

$$M = \frac{n v_o}{v_i} = \frac{1}{1 - \frac{\pi^2}{4k} \left(\frac{f_r}{f_s} - 1\right)}. \quad (13)$$

3. MOSFET ZVS Condition

The essence of ZVS in the power switch is to release the voltage V_{ds} on junction capacitances of the MOSFET to zero in the dead time of the circuit, then the drive signal V_{gs} of the MOSFET arrives, and ZVS is thereby achieved. The ZVS implementation of MOSFET includes the following three conditions:

- ZVS condition 1: The input impedance of the resonant network is inductive, which can ensure that the junction capacitor is discharged rather than charged. Additionally, the direction of the resonant current should not change during the dead time.

An LLC equivalent circuit considering the parasitic capacitance is shown in Figure 3.

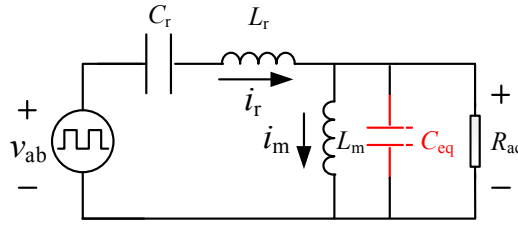


Figure 3. Equivalent circuit of an LLC resonant converter.

The impedance characteristics of the resonant tank are:

$$\begin{aligned} Z_{in} &= sL_r + \frac{1}{sC_r} + sL_m // \frac{1}{sC_{eq}} // R_{ac} \\ &= Z_0 \left\{ \frac{k^2 f^2 Q}{k^2 f^2 Q^2 + (kCf^2 - 1)^2} + j \left[f - \frac{1}{f} + \frac{kf - k^2 C f^3}{k^2 f^2 Q^2 + (kCf^2 - 1)^2} \right] \right\} \end{aligned} \quad (14)$$

where $Z_0 = \sqrt{L_r/C_r}$; $k = L_m/L_r$ represents the inductance coefficient; $Q = \frac{\omega_r L_r}{R_{ac}} = \frac{1}{R_{ac}} \sqrt{\frac{L_r}{C_r}}$ represents the quality factor; $f_r = \frac{1}{2\pi\sqrt{L_r C_r}}$ represents the resonant frequency; $f = \frac{f_s}{f_r}$ represents the normalized frequency; $C = \frac{C_{eq}}{C_r}$ represents the normalized equivalent capacitance; and C_{eq} represents the parasitic capacitance equivalent to the primary side. When the imaginary part is zero, the boundary point where the impedance characteristic lies between the inductive and capacitive states can be obtained.

$$f - \frac{1}{f} + \frac{kf - k^2 C f^3}{k^2 f^2 Q^2 + (kCf^2 - 1)^2} = 0 \quad (15)$$

The following can be derived:

$$Q_{\max}(f, k) = \sqrt{\frac{kCf^2 - 1}{k(f^2 - 1)} - \frac{(kCf^2 - 1)^2}{k^2 f^2}}. \quad (16)$$

The following can be obtained:

$$Q = \frac{2\pi f_r L_r}{R_{ac}} = \frac{2\pi f_r L_m}{k R_{ac}} < 0.95 Q_{\max}(f, k) = \sqrt{\frac{kCf^2 - 1}{k(f^2 - 1)} - \frac{(kCf^2 - 1)^2}{k^2 f^2}} \quad (17)$$

$$L_m < 0.95 \frac{k R_{ac}}{2\pi f_r} \sqrt{\frac{kCf^2 - 1}{k(f^2 - 1)} - \frac{(kCf^2 - 1)^2}{k^2 f^2}}. \quad (18)$$

Q_{\max} represents the maximum Q that satisfies the inductive nature of the impedance. Usually, the design Q should have a margin of about 5%. Equation (18) is a necessary condition of ZVS, but this condition alone does not guarantee ZVS of the switch.

- ZVS condition 2: During the dead time, the resonant current must be large enough to discharge the junction capacitor voltage of the MOSFET to zero. During the entire dead time, the discharge current cannot be changed in direction. Otherwise, the junction capacitance of the MOSFET will be recharged after being discharged.

As can be seen from Figure 2a, the current of the secondary side is zero when MOSFETs on the primary side turn off, i.e., $i_r = i_m$. Additionally, the magnetizing current reaches a peak, which is the discharging current of MOSFET junction capacitance as illustrated in Equation (3). During dead time, the resonant current not only fills the junction capacitance of the MOSFETs, but also changes the

voltage across the parasitic capacitance from nv_o to $-nv_o$. The minimum resonant current that satisfies the conditions is:

$$I_{\min} = 4C_{oss} \frac{v_i}{T_d} + 2C_{eq} \frac{nv_o}{T_d} \quad (19)$$

where C_{oss} represents the output capacitance of the MOSFET and T_d represents the dead time. Another necessary condition for achieving ZVS is:

$$I_{\min} < \frac{nv_o}{4f_r L_m}, \quad (20)$$

i.e.,

$$L_m < \frac{nv_o}{4f_r I_{\min}}. \quad (21)$$

- ZVS condition 3: Impedance angle

Even if the above two necessary conditions are satisfied, it is also necessary to determine whether ZVS is achieved by checking the value θ of Equation (8). If the impedance angle is too small, it means that the resonant circuit operates near the critical area of the inductive and capacitive state, which is dangerous for the converter.

As can be seen from Equation (8), θ gets the minimal value when $f_s = f_{\min}$ and I_o is the largest. At this operating point, it is the hardest to achieve soft switching. Under the condition that the parasitic capacitance is fully discharged in the dead time, ZVS can be achieved over the entire output voltage range as long as the operating point is guaranteed to be soft-switched. To ensure ZVS when the output is fully loaded at the minimum operating frequency, the resonant current should not reverse during the dead time, i.e. $\theta \geq 2\pi f_r T_d$. The body diode of the switch should be conducted before the drive signal arrives. It can be derived from $\theta \geq 2\pi f_r T_d$ and Equation (8):

$$L_m \leq \frac{n^2 v_o}{2\pi f_r I_o \tan(2\pi f_r T_d)} \cdot \frac{f_s}{f_r}. \quad (22)$$

When the converter is operating at the minimum frequency with full load ($f_s = f_{\min}$, $I_o = I_{o,\max}$), the critical value of the magnetizing inductance is:

$$L_m \leq \frac{n^2 R}{2\pi f_r \tan(2\pi f_r T_d)} \cdot \frac{f_{\min}}{f_r} \quad (23)$$

where R represents the direct current (DC) equivalent resistance under a full-load condition; and f_{\min} represents the minimum operating frequency. An LLC resonant converter's design should meet the highest gain at a minimum-frequency, full-load condition, i.e.,

$$M|_{f_{\min}} \geq M_{\max}. \quad (24)$$

The three conditions for achieving ZVS from full-load to no-load conditions are Equations (18), (21) and (23).

4. Optimal Design of LLC Resonant Converter Parameters

The goal of the LLC resonant converter's design is to select a set of parameters that can achieve high efficiency while meeting the output voltage and power requirements. This paper presents an optimal design method for LLC resonant converter parameters that can meet the gain requirement and ensure high efficiency at the same time. The converter parameters required are shown as follows:

- (1) Rated output power $P_o = 150$ W; and
- (2) Input voltage $v_i = 100$ V; rated output voltage $v_o = 30$ V; Output voltage range $v_{o,\min} - v_{o,\max} = 24 - 48$ V.

The maximum and minimum normalized gains of the LLC resonant converter are:

$$M_{\max} = \frac{nv_{o\max}}{v_i} \quad (25)$$

$$M_{\min} = \frac{nv_{o\min}}{v_i}. \quad (26)$$

4.1. Loss and Efficiency Analysis

When the LLC resonant converter is in operation, its power losses mainly include primary power switch losses P_p ; synchronous rectifier losses P_s on the secondary side; resonant inductance losses P_{Lr} ; and transformer losses P_T . The total loss and efficiency of the converter can be obtained as [20–23]

$$P_{\text{loss}} = P_p + P_s + P_{Lr} + P_T \\ = I_{r,RMS}^2(2R_{ds} + R_{Lr} + R_{T,p}) + I_{s,RMS}^2 R_{T,s} + \frac{I_m^2 t_f^2 f}{24C_{oss}} + P_s + k_{Lr} f^{\alpha_{Lr}} (\mu_{Lr} \frac{N_{Lr} l_r}{l_{Lr}})^{\beta_{Lr}} V_{Lr} + k_T f^{\alpha_T} (\mu_T \frac{N_p l_m}{l_T})^{\beta_T} V_T \quad (27)$$

$$\eta = \frac{P_o}{P_o + P_{\text{loss}}} \quad (28)$$

where C_{oss} represents the output capacitance of the MOSFET; t_f represents drop time of the switching off current; the subscripts L_r and T represent the resonant inductance and transformer, respectively; N represents the number of turns of the inductor coil; μ represents the magnetic permeability; l represents the magnetic circuit length; f represents the operating frequency; V represents the core volume; k represents the core loss coefficient; $\alpha = 1.5\text{--}1.7$ represents the frequency loss index; $\beta = 2\text{--}2.7$ represents the magnetic loss index; and k , α , and β can be obtained by consulting the relevant core manual to get its specific value.

When $P_o = 150$ W, $v_o = 30$ V, and $v_i = 100$ V, the relationship of P_{loss} , η versus f , and L_m is indicated in Figure 4a,b, respectively. As can be seen from Figure 4, the efficiency of the converter gradually increases as f and L_m rise. However, the efficiency upper limit of the converter tends to be a constant after f and L_m reach a certain degree. The theoretical value of the efficiency has an upper limit. Therefore, the values of f and L_m need to be reasonably selected.

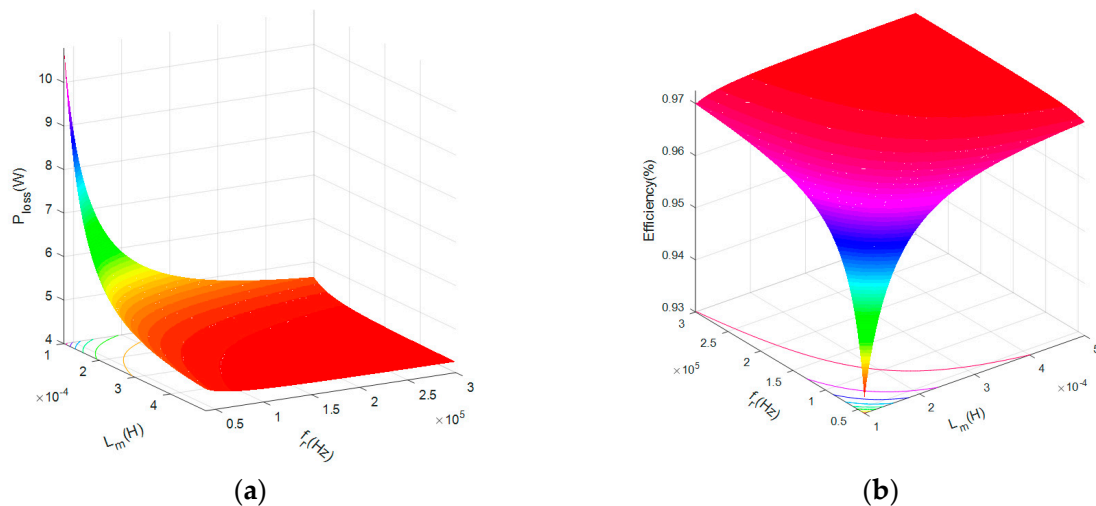


Figure 4. The relation of P_{loss} , η versus f and L_m : (a) P_{loss} ; (b) η .

4.2. Optimization Process

The overall design idea of this paper is illustrated in Figure 5, and the rated operating point is designed at the resonant frequency. At first, give the initial value of f_{\min} , and then calculate k

satisfying the gain required according to Equations (13) and (25). According to Equation (18), k can be converted to the constraint of ZVS. Based on the three ZVS constraints and the efficiency requirements, the intersection of the optimal design can be obtained to select an appropriate f_r and L_m so that L_r and C_r can also be determined. If the intersection does not exist, the efficiency or f_{min} can be appropriately reduced to obtain the parameters.

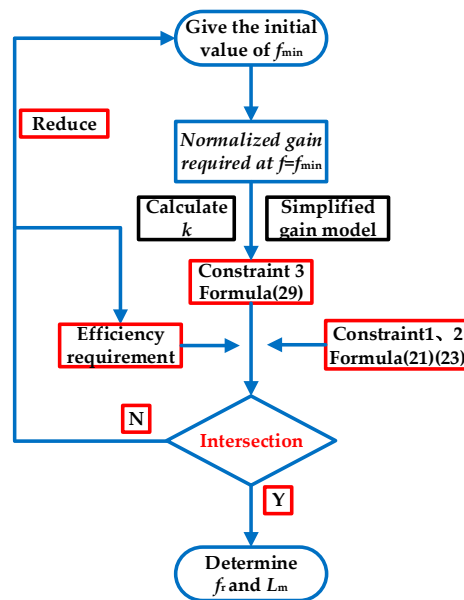


Figure 5. Flow chart for the optimal design of the parameters.

To limit the frequency to a small range, $f_{min} = 0.8f_r$ is initially taken. When $f = f_{min}$, the gain curve can be obtained from Equation (13) as displayed in Figure 6, where M represents the normalized voltage gain and it can be obtained from Equations (24) and (25) that $k \leq 1.6454$. The critical point is shown in Figure 6.

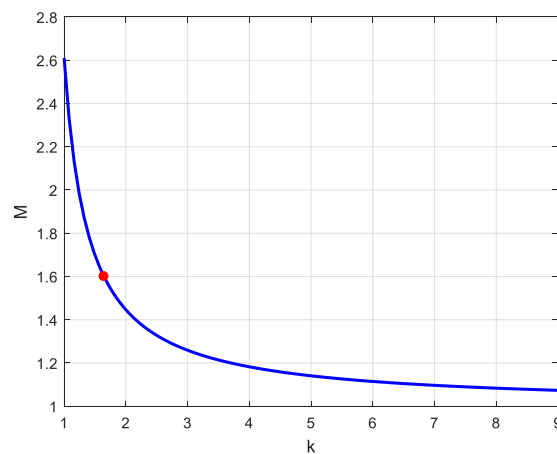


Figure 6. Simplified time-domain gain curves of different k values in PO mode.

When $f = f_{min} = 0.8f_r$, the function curve in Equation (18) is shown in Figure 7. As can be seen from the figure, the value gradually increases as k increases.

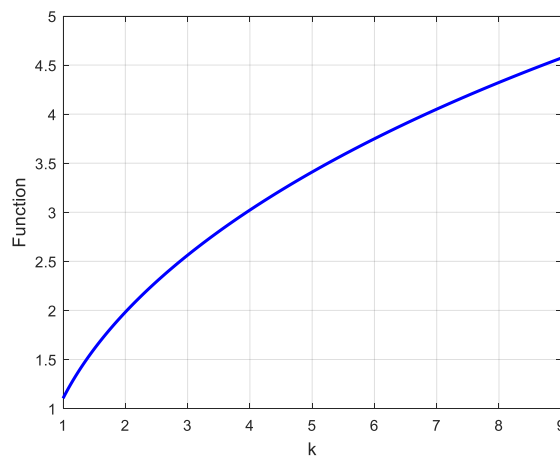


Figure 7. Function curve of $k\sqrt{\frac{kCf^2-1}{k(f^2-1)} - \frac{(kCf^2-1)^2}{k^2f^2}}$.

The required maximum normalized voltage gain $M_{\max} \geq 1.6$ ($k \leq 1.6454$), where Equation (18) is equivalent to Equation (29).

$$\frac{2\pi f_r L_m}{R_{ac}} < 0.95 \max\left(k\sqrt{\frac{kCf^2-1}{k(f^2-1)} - \frac{(kCf^2-1)^2}{k^2f^2}}\right) = 0.95k\sqrt{\frac{kCf^2-1}{k(f^2-1)} - \frac{(kCf^2-1)^2}{k^2f^2}} \Bigg|_{k=1.6454} \quad (29)$$

The three constraints for achieving ZVS from full-load to no-load conditions are Equations (21), (23) and (29). The optimal design of the parameters is actually the selection of parameters in intersecting regions of Equations (21), (23), (28) and (29). The intersection is shown in Figure 8 when the demand efficiency is set to be greater than 96.5%.

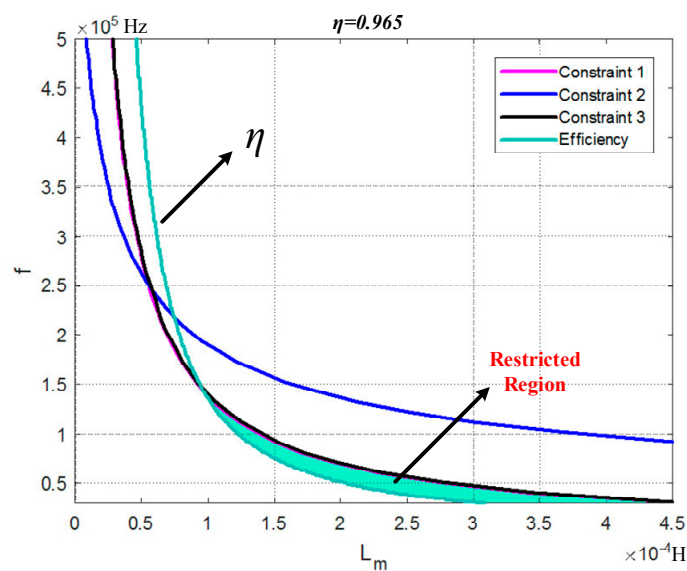


Figure 8. Intersection of ZVS constraints and efficiency requirement ($\eta > 96.5\%$).

When the expected efficiency increases, the efficiency curve shifts to the right. At the time, the intersection narrows or even disappears. When the expected efficiency decreases, the efficiency curve shifts to the left, and the intersection becomes larger as shown in Figure 9. As can be seen from Figure 9, the limited area will be very severe when the efficiency demand is relatively large. Moreover,

the resonance frequency in the restricted area is too small, which is detrimental to the volume reduction and high power density of the LLC resonant converter.

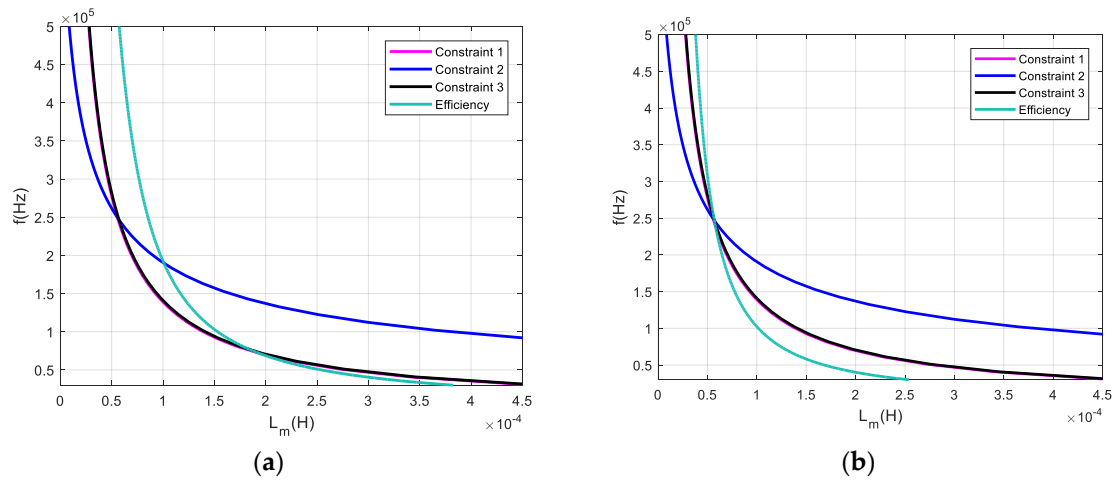


Figure 9. Influence of expected efficiency on the restricted design area of the converter: (a) Increased efficiency; (b) Decreased efficiency.

Based on the above analysis, the parameters of the converter selected in the intersecting area in Figure 8 are shown in Table 1. The loss composition analysis is performed according to the parameters as is indicated in Figure 10. The results show that the conduction loss and turn-off loss of MOSFETs on the primary side and the on-state switching loss on the secondary side account for the majority of the total losses. The on-state switching loss on the secondary side accounts for 58% of the total losses. The iron loss of the transformer and the inductor accounts for less than 1%; thus, they are not shown in the figure.

Table 1. Optimal parameters of the LLC resonant converter.

Parameter	Value
Input voltage	100 V
Rated Output voltage	30 V
Rated power	150 W
Transformer ratio	10:3
Resonant inductor	85.1 μ H
Resonant capacitor	36.7 nF
Magnetic inductor	140 μ H
Output capacitor	1000 μ F

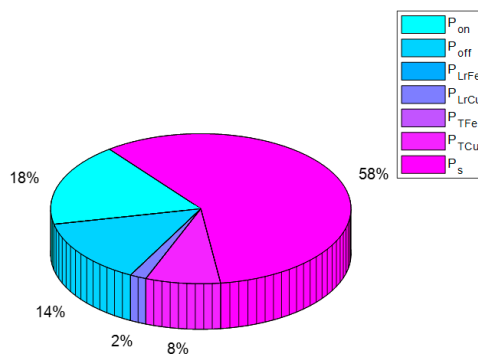


Figure 10. Loss composition analysis of the LLC resonant converter.

5. Simulation and Experiments

- (1) Simulation

The parameters in Table 1 are verified by simulation, and the results are shown in Figures 11 and 12. The waveforms under different load conditions at the resonant frequency are shown in Figure 11. As can be seen from Figure 11, ZVS on the primary side can be achieved from a full-load to a no-load condition when $f = f_r$, which proves the effectiveness of the proposed method. The next step is to verify the gain requirement at $f = 0.8 f_r = 72$ kHz; the simulation results are shown in Figure 12.

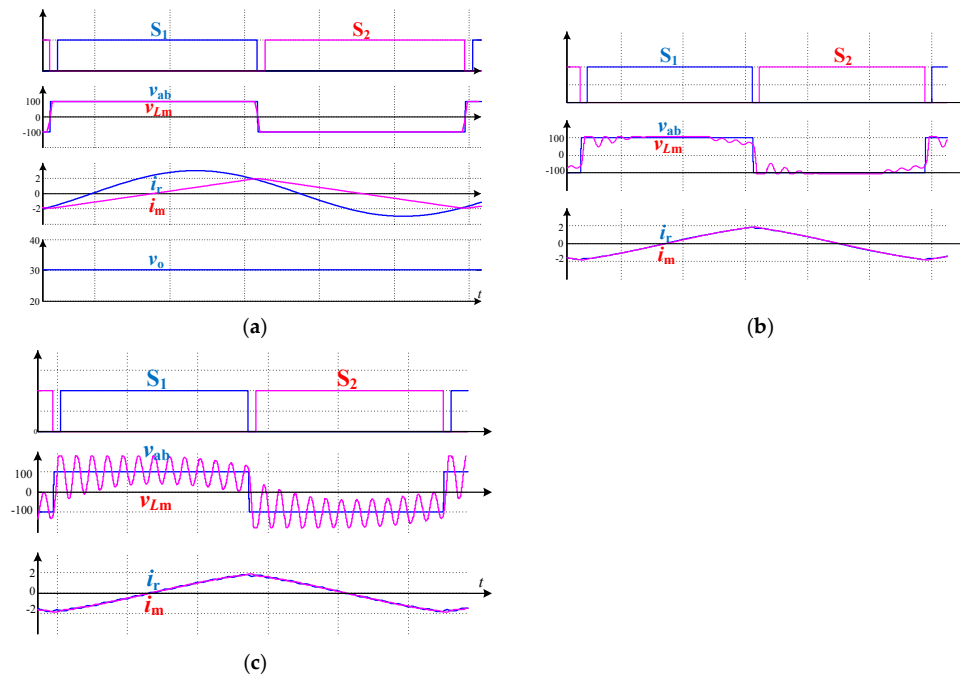


Figure 11. Simulation waveforms under different loads ($f = f_r$): (a) full load; (b) 1% rated load; (c) no load.

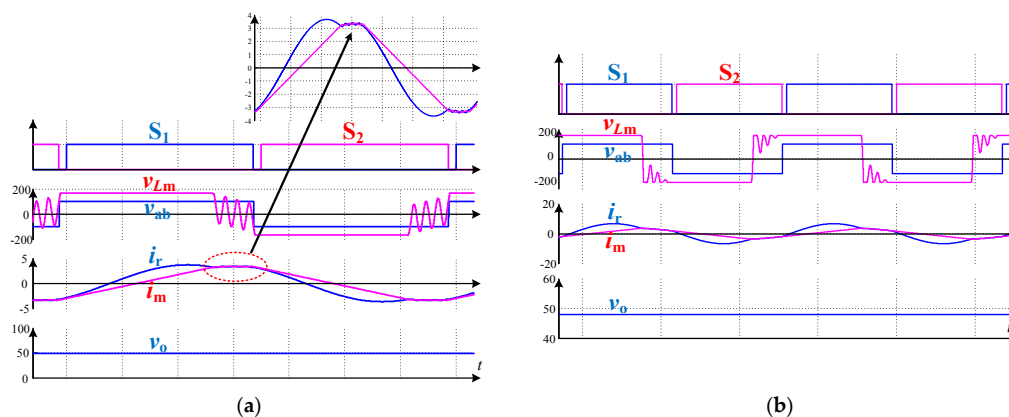


Figure 12. Simulation waveforms under different loads ($f = 0.8f_r$): (a) full load ($P = 150$ W); (b) heavy load ($R = 6, P = 384$ W).

As is displayed Figure 12a, the waveform under a full-load condition is nearly consistent with the simplified gain analysis model described above. Although the waveforms of the resonant current and the magnetizing current in Figure 12b have a small deviation from the simplified gain model, it has little effect on the gain calculation. As can be seen from Figure 12b, soft switching can still be

achieved under a heavy load condition ($R = 6$, output power is $P_{max} = 384 \text{ W} >$ rated power 150 W) while satisfying the required voltage gain. Additionally, the minimum voltage of 24 V can be obtained at about 106 kHz .

- (2) Experiments

The practicability and effectiveness of the proposed method are further verified through experiments. The prototype of the experimental setup is shown in Figure 13. The experimental results are shown in Figures 14–17, where Figure 14 is the experimental waveform under different load conditions at the resonant frequency.

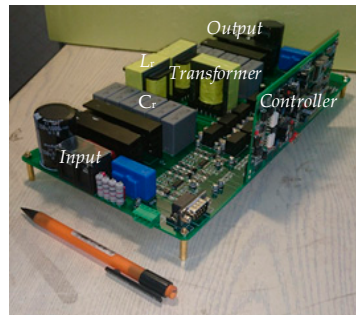
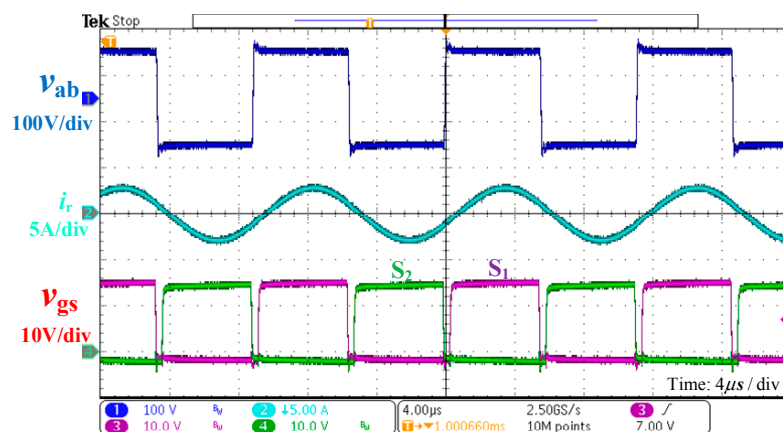
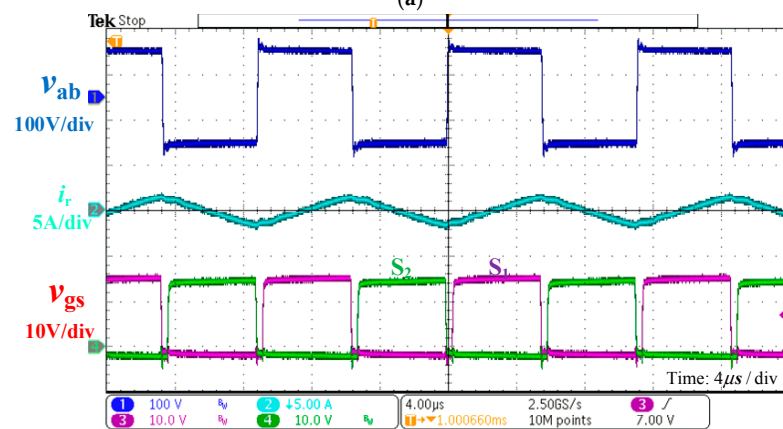


Figure 13. The prototype of the experimental setup.



(a)



(b)

Figure 14. Cont.

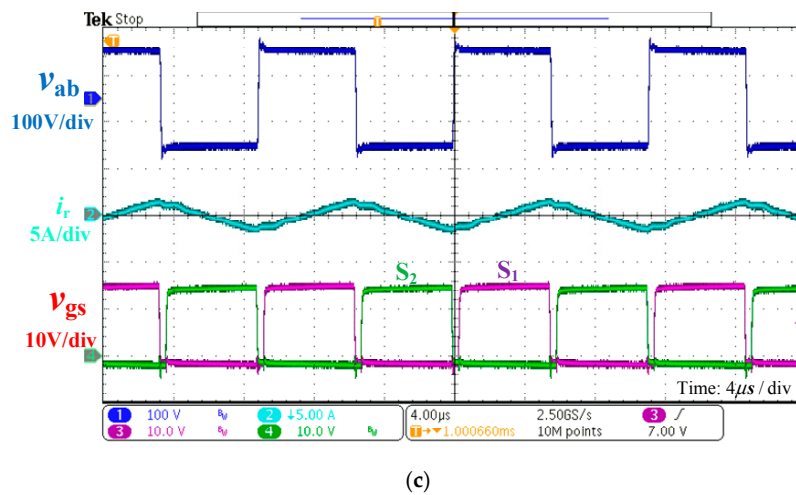


Figure 14. Experimental waveforms under different loads ($f = f_r$): (a) full load; (b) 1% rated load; (c) no load.

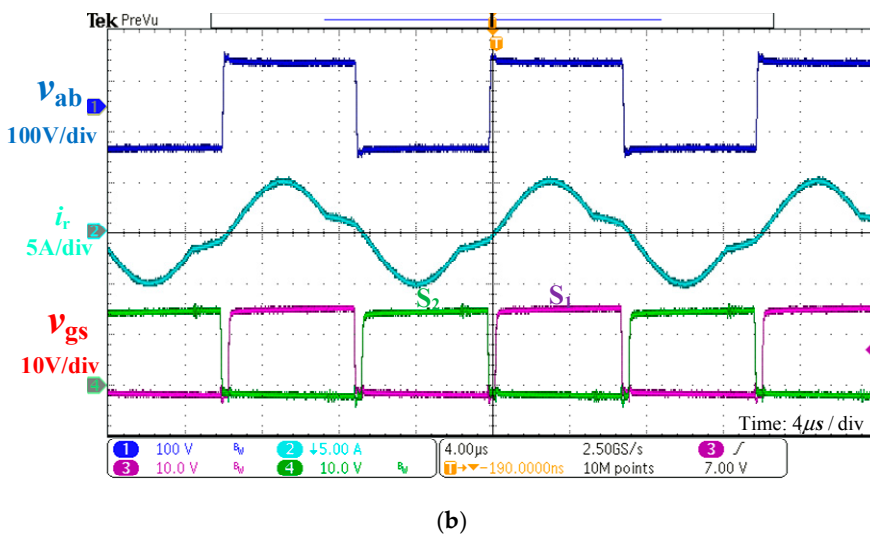
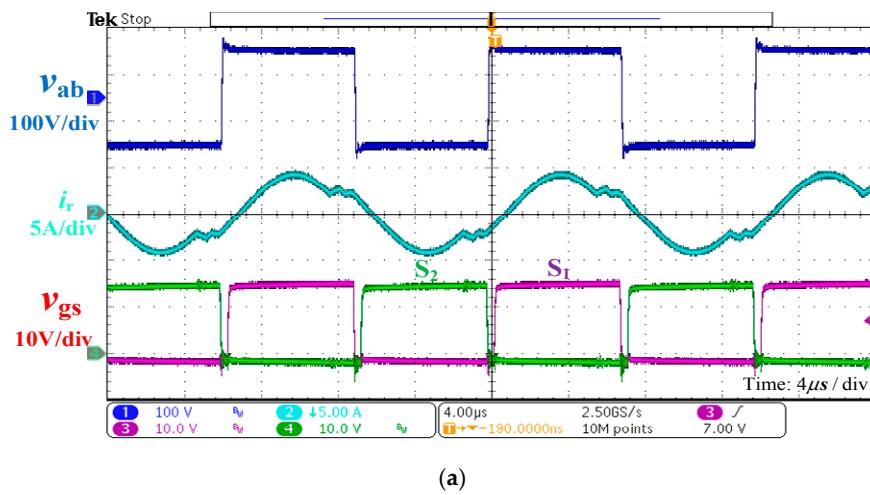


Figure 15. Experimental waveforms under different loads ($f = 71.72$ kHz): (a) full load; (b) heavy load.

As is displayed in Figure 14, ZVS of the MOSFETs can be effectively achieved under all load conditions at the resonant frequency, which is consistent with the theoretical and simulation results. The fluctuation of the resonant current at a no-load condition in Figure 14c is caused by the charge and discharge effects of the parasitic capacitance.

Figure 15 shows the experimental waveforms under different load conditions when $f = 71.72$ kHz. As can be seen from Figure 15, the LLC resonant converter can effectively achieve ZVS under a rated load condition at f_{\min} ; the converter lies in a critical state under a heavy load condition, but ZVS can still be achieved. The fluctuation of resonant current at O mode in Figure 15a is also caused by the parasitic capacitance.

Gain curves of the designed LLC resonant converter obtained by FHA analysis, the simplified gain model, simulation, and experiment are compared in Figure 16, where f represents the normalized frequency. Figure 16 indicates that the gain curve obtained by FHA analysis has a relatively large discrepancy with the simulation and the experiment. The gain is smaller than the actual, and the gain obtained by the simplified gain model is very similar that obtained by the simulation and the experiment. It is relatively accurate to design the gain requirement of the converter by the simplified gain model in PO mode when the frequency variation range is very small.

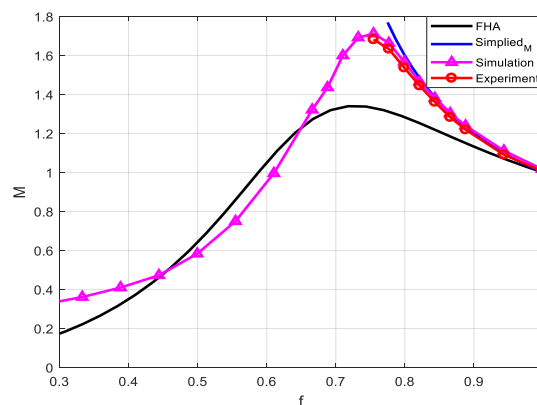


Figure 16. Gain curve comparison. FHA = fundamental harmonic approximation.

The measured efficiency curve is presented in the Figure 17. Under the medium and full-load conditions, the converter can maintain a high efficiency. The peak efficiency of the LLC resonant converter can reach about 96.3% when the output power is about 120 W. There is a small difference between the measured efficiency and the theory since the loss of the capacitor ESR and the layout resistance are not considered in the theoretical analysis. The efficiency varies with the input voltage, LLC power level, selection of MOSFET, and so on. It is not convenient to compare the efficiency with other methods under different conditions. Compared with the prototypes in studies [3,5,19,20] as shown in Table 2, the maximum normalized voltage gain and efficiency of the prototype in this paper are improved under a small power level. Moreover, the expected efficiency is adjustable, which means a converter with a higher efficiency can be designed as illustrated in Figure 9.

Table 2. Fair comparison to the other published methods.

Prototype	Efficiency	Power	Maximum Normalized Voltage Gain	Frequency Range
[3]	96.4%	350 W	1.2	45 kHz
[5]	95.5%	1.5 kW	1.67	30 kHz
[19]	98%	400 W	1.455	56 kHz
[20]	97.6%	3.3 kW	1.41	38 kHz
In this paper	96.3%	150 W	1.6	18 kHz

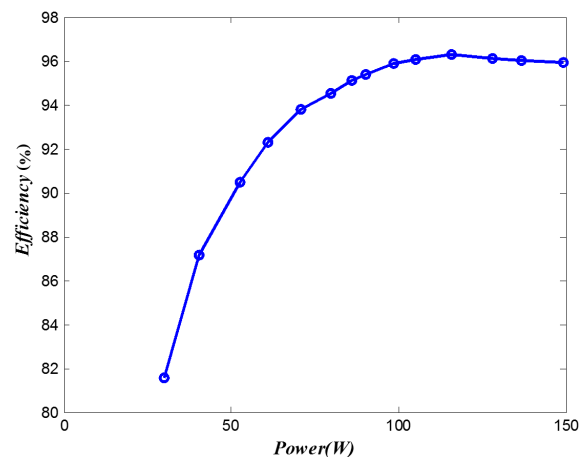


Figure 17. Measured efficiency curves.

6. Conclusions

This paper focused on the problem of the wide frequency regulating range in the design of voltage-adjustable LLC resonant converters and proposed an optimal design method, which can narrow the frequency range and ensure high efficiency of the converter under the premise of satisfying the required gain.

The proposed method is verified by simulation of and experiment using a 150 W prototype. The results show that the simplified gain model utilized has a relatively high degree of accuracy when the frequency variation range is very small, and ZVS can be effectively achieved from a no-load to a full-load and even a heavy-load condition. The method proposed in this paper can achieve 1.6 times the normalized voltage gain in the frequency variation range of 18 kHz with a peak efficiency of up to 96.3%. The maximum normalized voltage gain and efficiency of the prototype can maintain an excellent performance under a small power level. Moreover, the expected efficiency is adjustable, which means a converter with a higher efficiency can be designed. The method proposed in this paper can also be used for the design of large-power LLC resonant converters to obtain a wide output voltage range and higher efficiency.

Author Contributions: J.L. and J.W. conceived and designed the simulation and experiments; J.L. and Z.F. performed the experiments; J.S. and J.L. analyzed the data; J.L. wrote the paper.

Acknowledgments: This work was supported in part by the National Natural Science Foundation of China under the Project of 51707138 and 51507114 and in part by the National Key Research and Development Plan under the Project of 2017YFB1201002.

Conflicts of Interest: The authors declare no conflict of interest.

References

1. Fei, C.; Li, Q.; Lee, F.C. Digital Implementation of Adaptive Synchronous Rectifier (SR) Driving Scheme for High-Frequency LLC Converters With Microcontroller. *IEEE Trans. Power Electron.* **2018**, *33*, 5351–5361. [[CrossRef](#)]
2. Fang, Z.; Cai, T.; Duan, S.; Chen, C. Optimal design methodology for LLC resonant converter in battery charging applications based on time-weighted average efficiency. *IEEE Trans. Power Electron.* **2015**, *30*, 5469–5483. [[CrossRef](#)]
3. Kim, D.K.; Moon, S.C.; Yeon, C.O.; Moon, G.W. High-efficiency LLC resonant converter with high voltage gain using an auxiliary LC resonant circuit. *IEEE Trans. Power Electron.* **2016**, *31*, 6901–6909. [[CrossRef](#)]
4. Wang, H.; Li, Z. A PWM LLC type resonant converter adapted to wide output range in PEV charging applications. *IEEE Trans. Power Electron.* **2018**, *33*, 3791–3801. [[CrossRef](#)]

5. Wu, H.; Li, Y.; Xing, Y. LLC resonant converter with semiactive variable-structure rectifier (SA-VSR) for wide output voltage range application. *IEEE Trans. Power Electron.* **2016**, *31*, 3389–3394. [[CrossRef](#)]
6. Milan, M.J.; Irving, B.T. On-the-Fly Topology-Morphing Control—Efficiency Optimization Method for LLC Resonant Converters Operating in Wide Input- and/or Output-Voltage Range. *IEEE Trans. Power Electron.* **2015**, *31*, 2596–2608.
7. Kim, B.C.; Park, K.B.; Kim, C.E.; Lee, B.H.; Moon, G.W. LLC Resonant Converter With Adaptive Link-Voltage Variation for a High-Power-Density Adapter. *IEEE Trans. Power Electron.* **2010**, *25*, 2248–2252. [[CrossRef](#)]
8. Kim, J.W.; Moon, G.W. A new LLC series resonant converter with a narrow switching frequency variation and reduced conduction losses. *IEEE Trans. Power Electron.* **2014**, *29*, 4278–4287. [[CrossRef](#)]
9. Qian, Q.; Yu, J.; Su, C.; Sun, W.; Lu, W. A LLC resonant converter with dual resonant frequency for high light load efficiency. *Int. J. Electron.* **2017**, *104*, 2033–2047. [[CrossRef](#)]
10. Fei, C.; Lee, F.C.; Li, Q. Digital implementation of soft start-up and short-circuit protection for high-frequency LLC converters with optimal trajectory control (OTC). *IEEE Trans. Power Electron.* **2017**, *32*, 8008–8017. [[CrossRef](#)]
11. Zheng, R.; Liu, B.; Duan, S. Analysis and parameter optimization of start-up process for LLC resonant converter. *IEEE Trans. Power Electron.* **2015**, *30*, 7113–7122. [[CrossRef](#)]
12. Hu, Z.; Wang, L.; Wang, H.; Liu, Y.; Sen, P.C. An accurate design algorithm for LLC resonant converters—Part I. *IEEE Trans. Power Electron.* **2016**, *31*, 5435–5447. [[CrossRef](#)]
13. Hu, Z.; Wang, L.; Qiu, Y.; Liu, Y.; Sen, P.C. An accurate design algorithm for LLC resonant converters—Part II. *IEEE Trans. Power Electron.* **2016**, *31*, 5448–5460. [[CrossRef](#)]
14. Fang, X.; Hu, H.; Shen, Z.J.; Batarseh, I. Operation Mode Analysis and Peak Gain Approximation of the LLC Resonant Converter. *IEEE Trans. Power Electron.* **2012**, *27*, 1985–1995. [[CrossRef](#)]
15. Yu, R.; Ho, G.K.Y.; Pong, B.M.H.; Ling, B.W.K.; Lam, J. Computer-Aided Design and Optimization of High-Efficiency LLC Series Resonant Converter. *IEEE Trans. Power Electron.* **2012**, *27*, 3243–3256. [[CrossRef](#)]
16. Musavi, F.; Craciun, M.; Gautam, D.S.; Eberle, W.; Dunford, W.G. An LLC resonant DC–DC converter for wide output voltage range battery charging applications. *IEEE Trans. Power Electron.* **2013**, *28*, 5437–5445. [[CrossRef](#)]
17. Deng, J.; Mi, C.C.; Ma, R.; Li, S. Design of LLC resonant converters based on operation-mode analysis for level two PHEV battery chargers. *IEEE/ASME Trans. Mechatron.* **2015**, *20*, 1595–1606. [[CrossRef](#)]
18. Hu, H.; Fang, X.; Chen, F.; Shen, Z.J.; Batarseh, I. A modified high-efficiency LLC converter with two transformers for wide input-voltage range applications. *IEEE Trans. Power Electron.* **2013**, *28*, 1946–1960. [[CrossRef](#)]
19. Fang, X.; Hu, H.; Chen, F.; Somani, U.; Auadisiyan, E.; Shen, J.; Batarseh, I. Efficiency-oriented optimal design of the LLC resonant converter based on peak gain placement. *IEEE Trans. Power Electron.* **2013**, *28*, 2285–2296. [[CrossRef](#)]
20. Xu, H.; Yin, Z.; Zhao, Y.; Huang, Y. Accurate Design of High-Efficiency LLC Resonant Converter with Wide Output Voltage. *IEEE Access* **2017**, *5*, 26653–26665. [[CrossRef](#)]
21. Zhansong, Z.; Xuansan, C. *The Principles and Design of Switching Power Supply*; Electronics Industry Press: Beijing, China, 1999. (In Chinese)
22. Xiuke, Z. *Magnetic Components in Switching Power Supplies*; Liaoning Science and Technology Press: Shenyang, China, 2004. (In Chinese)
23. Hurley, W.G.; Wölfle, W.H. *Transformers and Inductors for Power Electronics: Theory, Design and Applications*; John Wiley & Sons Ltd.: Chichester, UK, 2013.

